Examination of depth-weighted optical signals during cardiac optical mapping: A simulation study

Zhenghong Xu[a,b], Zhenxi Zhang[a,*], Yinbin Jin[a,b], Jing Wang[a]

[a]*The key Laboratory of Biomedical Information Engineering of Education Ministry, The School of Life Science and Technology, Xi'an Jiaotong University, Xi'an 710049, PR China*
[b]*The School of Electrical Engineering, Xi'an Jiaotong University, Xi'an 710049, PR China*

Abstract

Optical mapping has become a powerful tool to explore complex cardiac propagation. Many experiments and studies claimed that the fluorescence obtained from tissue surface is the averaged response of the transmembrane potential upon probing depth rather than only on the surface. With the electrical propagation model and the photon transport model, the effects of depth-weighted optical signals are examined both during a normal excitation wave and a spiral wave. Our results indicate that depth-weighted optical signals may infer cardiac activation dynamics, such as the mode and the direction of the propagation, the spatial distribution of depolarization or repolarization.
© 2006 Elsevier Ltd. All rights reserved.

Keywords: Optical mapping; Fluorescence; Computer simulation; Cardiac electrophysiology

1. Introduction

Sudden cardiac death due to ventricular arrhythmias is a major public problem, resulting in more than 450,000 deaths annually in the United States [1]. Quantification of the spatial and temporal dynamics of propagating waves of cardiac electrical activities is very important to explore the mechanisms of arrhythmias and defibrillation. Since 1990s, optical mapping with voltage-sensitive dyes has become a powerful tool and has been widely applied to unsolvable problems of cardiac electrophysiology and it can "image" electrical activity in a wide range, from the level of cellular to the whole heart [1–3]. In normal optical mapping in an epi-illumination mode, the light source and photo detector are placed above the epicardium [3–6]. So it is largely limited to two-dimensional measurements and it records changed intensity of fluorescence only from the tissue surface.

Several experiments and studies have pointed out that optical signal should not be compared to the transmembrane potential at the tissue surface [3,4,7]. The hypothetic reason is that optical signal presents an average fluorescent signal from the central depth rather than the surface of a tissue. The probing depth of a fluorescence measurement is defined as the depth above which mainly fluorescence originates. Different results have been reported. Baxter et al. [4] estimated that layers as deep as 2 mm beneath the surface might contribute to the optical signal. Efimove et al. [5] and Chio et al. [8] reported the depth about 1–2 mm, but others such as Girouard et al. [9] predicted that 95% of the signal energy originates from a tissue depth of 0.5 mm or less and Knisley et al. [10] estimated that to be about 0.3 mm. Ding et al. [11] using Monte Carlo simulation indicated that 62% fluorescence originated within a block of tissue with 1 mm-radius and 1 mm depth. Differences in wavelengths, experimental preparations and dye concentrations used in experiments may lead to this discrepancy.

Our work is to establish the correlation between cardiac computer simulation and optical signal based on the theory of photon transport in tissue, to quantify the effects of the summation of the optical signals from layers and to determine the main factor affecting the discrepancy between the surface and depth-weighted signals. The

---

* Corresponding author. Tel.: +86 29 82666854; fax: +86 29 82663927.
E-mail address: zxzhang@mail.xjtu.edu.cn (Zhenxi Zhang).

computational model we present in this study consists of two parts: a model of electrical transmural propagation and a model of photon transport. The two models are then combined to simulate the optical signal detected from tissue surface with an epi-illumination mode that is commonly used in cardiac optical mapping.

2. Method

2.1. Electrical transmural propagation model

The Luo–Rudy ionic model of mammalian ventricular cell is used in the 2-D (two-dimension) cardiac tissue to simulate the distribution of the transmembrane potential (V) [12]. A Cartesian co-ordinate is employed here, X is along the tissue surface and Z is the depth below. The transmural tissue includes epicardium, midmyocardial cell (M cell) and endocardium from the top to the bottom. Excitation wave propagation in 2-D virtual ventricular tissue is described by the reaction–diffusion-like equation with no-flux boundary conditions

$$C_{\mathrm{m}} \frac{\partial V}{\partial t} = -I_{\mathrm{ion}} + \frac{1}{\rho_x S_{\mathrm{v}}} \frac{\partial^2 V}{\partial x^2} + \frac{1}{\rho_z S_{\mathrm{v}}} \frac{\partial^2 V}{\partial z^2}, \tag{1}$$

where C_{m} is the membrane capacitance, S_{v} is the surface-to-volume ratio, ρ_x and ρ_z are the transverse and longitudinal resistivities, V is the transmembrane potential and t is the time. The ionic current I_{ion} is taken from [12].

2.2. Photon transport model

The photon transport model is used to estimate the non-uniform contributions of different tissue layers to the total fluorescence escaping from surface with an epi-illumination mode. We assume that: (1) the tissue is optically homogeneous and fluorescence is emitted isotropically from different depths; and (2) the scatting loss of escaped fluorescence at tissue surface is ignored because the fraction of the fluorescence signal originated at a given depth in the tissue does not depend on the radius of image array element [11].

Based on diffusion theory, light transports away from the source approximatively followed by an exponential delay. The distributions of excitation and emission light in biology tissue have been described by the accurate expressions for one-dimensional fluence rate $\Phi(\mathrm{W/m}^2)$ and escape function $G(\mathrm{W/m}^2)$ as follows [13]:

$$\Phi(z) = C_1 \exp(-k_1 z/\delta_{\mathrm{ex}}) - C_2 \exp(-k_2 z/\delta_{\mathrm{ex}}), \tag{2}$$

$$G(z) = C_3 \exp(-k_3 z/\delta_{\mathrm{f}}), \tag{3}$$

where z is the depth beneath the surface. $\Phi(z)$ is the intensity of excitation light with depth z. Eq. (2) has a second exponential term to account for photons scatting out of the tissue near the surface. δ_{ex} is the penetration depth for excitation light. The escape function $G(z)$ represents the intensity of fluorescence escaping from a certain z to the tissue

surface and δ_{f} is the penetration depth for escape fluorescence. The parameters C_1, k_1, C_2, k_2, C_3 and k_3 are free variable and can be determined by experimental measurement and data fitting.

The weighting function $w(z)$ used to estimate the fluorescence contributions of different layers to the total fluorescence escaping from surface is given by

$$w(z) = \Phi(z)G(z / \int_0^Z \Phi(z)G(z)\,\mathrm{d}z, \tag{4}$$

where Z is the maximal depth of photon transport model and z is the depth beneath the surface.

2.3. Depth-weighted optical signal

The electrical propagation model and photon transport model are combined to calculate the depth-weighted optical signal. We assume that: (1) the fluorescence intensity is the instantaneous response to the change of transmembrane potential because the velocity of fluorescence is far more rapidly than the speed of the electrical conduction (about 0.5 m/s); and (2) the distribution and properties of the voltage-sensitive dye are uniform throughout the tissue. The depth-dependent optical signal which equals to the intensity of fluorescence captured from the surface, is given by

$$\bar{V}(x) = \int_0^Z V_{\mathrm{m}}(x, z)w(z)\,\mathrm{d}z, \tag{5}$$

where V_{m} represents deviation of the transmembrane potential (obtained by Eq. (1)) from the resting membrane potential ($V_{\mathrm{m}} = V - V_{\mathrm{rest}}$). Z is the maximal depth of photon transport model, and z is the depth beneath the surface and $z = 0$ denotes the illuminated surface.

2.4. Simulation design

We simulate the electrical transmural propagation in a 1.5 cm × 1.5 cm (100 × 100 nodes) slab of tissue, as shown in Fig. 1(a). The Eq. (1) is solved according to the time splitting method [14]. Here $C_{\mathrm{m}} = 1\,\mu\mathrm{F/cm}^2$, $S_{\mathrm{v}} = 2000\,\mathrm{cm}^{-1}$, $\rho_x = \rho_z = 0.5\,\mathrm{k}\Omega\,\mathrm{cm}$. The spatial step size is set to 0.015 cm and the adaptive temporal step is 0.01–0.1 ms. This numerical simulation is implemented on a Pentium Pro (2.4 GHz) PC by using programs we have developed in Fortran90 [15].

We analyzed the electrical propagation both under a normal impulse and a reentrant impulse. A normal excitation wave is initiated by uniplor stimulus S_1 at the endocardial side with 0.5 ms duration and $-80\,\mu\mathrm{A/cm}^{-2}$ current. The spherical wave spreads from the bottom to the top. We intend to emulate the normal excitation wave from an endocardium- M cell- epicardium path is similar to the propagation of real hearts. The transmural reentrant wave is initiated by the stimulus S_2 (parameters are the same as S_1) at the epicardial side which is added at an appropriate time and is felicitously formed a spiral wave. During reentry, the spiral wave propagates back into a previously depolarized area that has recovered excitability
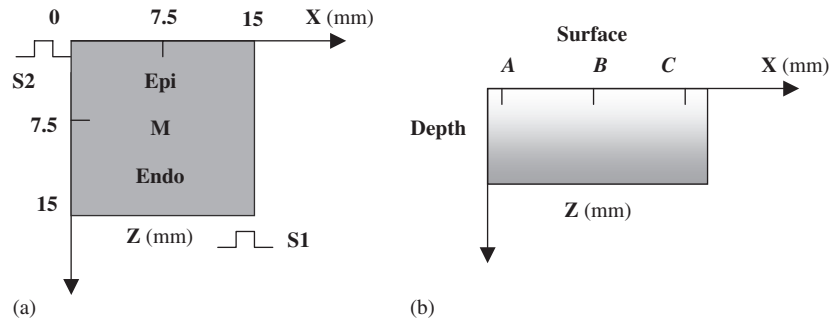
Fig. 1. A sketch of the models. Here x runs parallel to the tissue surface and z is the depth below: (a) is electrical transmural propagation model. A normal excitation wave was initiated by unipolar stimulation S_1. After that a S_2 stimulation was added at a correctly time and felicitously formed a spiral wave. Epi indicates epicardium; M, Midmyocardial cells; Endo, endocardium and (b) is photon transport model. Three points A, B and C on the surface are chosen to analyze the position influence.

and then the activation pattern changed. The wave is rotating anticlockwise continuously and the reentrant core is near the central tissue.

Simulation in light transport model is only with dimensions $1.5\,\text{cm} \times 0.8\,\text{cm}$, as shown in Fig. 1(b). $\Phi(z)$ and $G(z)$ we used are determined by experimental measurement and data fitting as shown in [4] considering scattering losses of excitation light at the tissue surface,

$$\Phi(z)G(z) = (927\mathrm{e}^{-z/0.8} - 702\mathrm{e}^{-z/0.44})\mathrm{e}^{-z/1.34}. \qquad (6)$$

Light attenuation in tissue mostly depends on depths. If the tissue is thicker than $0.8\,\text{cm}$, the contribution of fluorescence remains essentially unchanged and little enough to be negligible [4]. Removing the data beyond $0.8\,\text{cm}$ would not affect the accuracy and could reduce the calculation time. The three points of A, B and C on the surface are chosen to analyze the position influence. Moreover, we use V_0 to refer to the values of V_m located at the top layer and $\bar{V}$ to represent the signal derived from depth-weighted average of V_m.

3. Results

3.1. Effect of propagation mode

The action potentials of V_0 and $\bar{V}$ are calculated at the points of A, B and C on surface during a normal excitation wave and a spiral wave. The morphology of $\bar{V}$ and V_0 at different points are nearly superposition during normal excitation wave, as is shown in Fig. 2(a), but $\bar{V}$ upstroke initiates a little bit earlier than V_0 because the intramural cells depolarize previously and their potentials are appreciably higher. When cells on the surface are on the resting membrane potential, $\bar{V}$ is higher than V_0 and the whole APD (action potential duration) of $\bar{V}$ is longer than that of V_0. Because tissue includes M cells and their APDs are relatively longer (30–40 ms) compared with cells of epicardium and endocardium [16], the cells of top layer repolarize earlier than the intramural cells. Summarily there is a few differences between $\bar{V}$ and V_0 during normal excitation

wave. The morphology of $\bar{V}$ is independent of the position on surface.

When spiral wave occurs, the differences between $\bar{V}$ and V_0 are obviously greater than that during a normal excitation wave, as is shown in Fig. 2(b). The upstroke morphology of $\bar{V}$ is different from points A, B and C and will be described in Section 3.3. The repolarization traces of $\bar{V}$ are nearly the same as that during the normal excitation wave because of the long-APD influence of M cells. At point B, the peak of $\bar{V}$ noticeably is lower in amplitude than that of V_0. The morphology of $\bar{V}$ is clearly dependent upon the position on surface during a spiral wave.

3.2. Effect of wave front

Traces of the V_0 and $\bar{V}$ along X-axes with the respective gray-scale images are shown in Fig. 3. The gradient of gray expresses the corresponding transmembrane potential (V_m) in tissue (data are normalized to the maximum value). We observe that $\bar{V}$ is greater than V_0 only in the regions where the wave fronts toward the surface, such as in Fig. 3(a). As the spiral wave progresses anticlockwise, when wave fronts are traveling away from the tissue surface $\bar{V}$ is lower in magnitude than V_0 due to the higher transmembrane potential on surface cells comparing to the intramural cells, as is shown in Fig. 3(b). But $\bar{V}$ is equal to V_0 only in the region where wave fronts are parallel to the surface, such as the middle zone in Fig. 3(c). The difference between $\bar{V}$ and V_0 is significantly correlated to the direction of the wave front.

3.3. Upstroke morphology of depth-weighted optical signal

The upstroke morphologies of $\bar{V}$ during spiral wave at points A, B and C are magnified in Fig. 4(a)–(c), respectively. And different morphologies are significantly dependent on the propagation directions as is shown in Fig. 4(d). The wave is rotating anticlockwise continuously and the core of the spiral wave is near the central tissue. So near point A, the wave fronts propagate away from surface and near point C the wave fronts propagate toward the surface. The point B is just above the core of
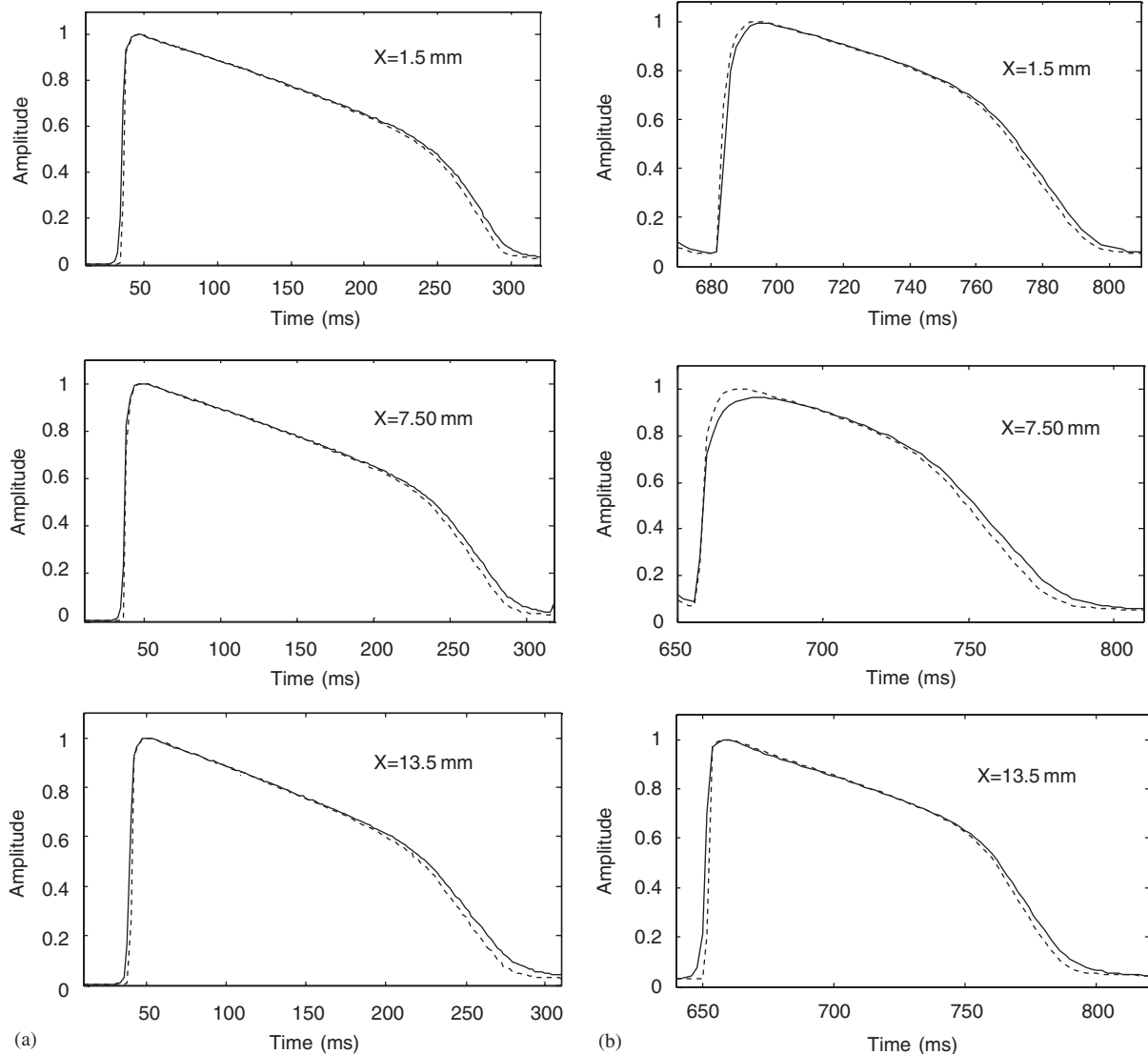
Fig. 2. Time traces of $\bar{V}$(black line) and V_0 (dotted line) at different points on surface during the normal excitation in (a) and that during the spiral wave in (b). The plots in (top), (middle) and (bottom) are obtained at point A ($x = 1.5$ mm), point B ($x = 7.50$ mm) and point C ($x = 13.5$ mm), respectively. Locations of points A, B and C are shown in Fig. 1(b).

spiral wave, so the wave fronts beneath the point B are nearly parallel to the surface. The upstroke morphology of $\bar{V}$ during the spiral wave at point C is the same as that during the normal excitation wave (see in Fig. 2(a)) due to the consistency of the propagation direction.

4. Discussion

Under the normal excitation wave the phase difference of action potential along depth is about 4 ms per 1.5 mm and the speed of the electrical conduction is about 0.375 m/s in our simulation. Wave propagation in tissue has the nearly consistent conduction velocity. So the phase differences of action potential between the top layer and the deep layer are same in tissue. Only a few differences appear between $\bar{V}$ and V_0 during normal excitation wave. But the conduction velocities differ at different

regions during a spiral wave. The apparent conduction velocity of outboard of spiral wave (the periphery of the tissue) is faster than that of the reentrant core (average 0.375 m/s vs. 0.125 m/s). The phase differences of the action potential between the top layer and the deep layer are increased near the reentrant core comparing to the other regions which far from the core. So the discrepancy of V_0 and $\bar{V}$ is dependent on the distribution of spiral wave. In conclusion, the inconsistent conduction velocity causes the increase of discrepancy in phases of action potential between the top layer and the deep layer during a spiral wave. It will be the main factor of the amplitude reduction of the depth-weighted signal close to the reentrant core.

The main goal of the present research is to obtain the solution of the so-called "forward problem" for the simulation of depth-dependent optical signal on the record-surface synthesized for a given 2-D electrical propagation. The photon transport
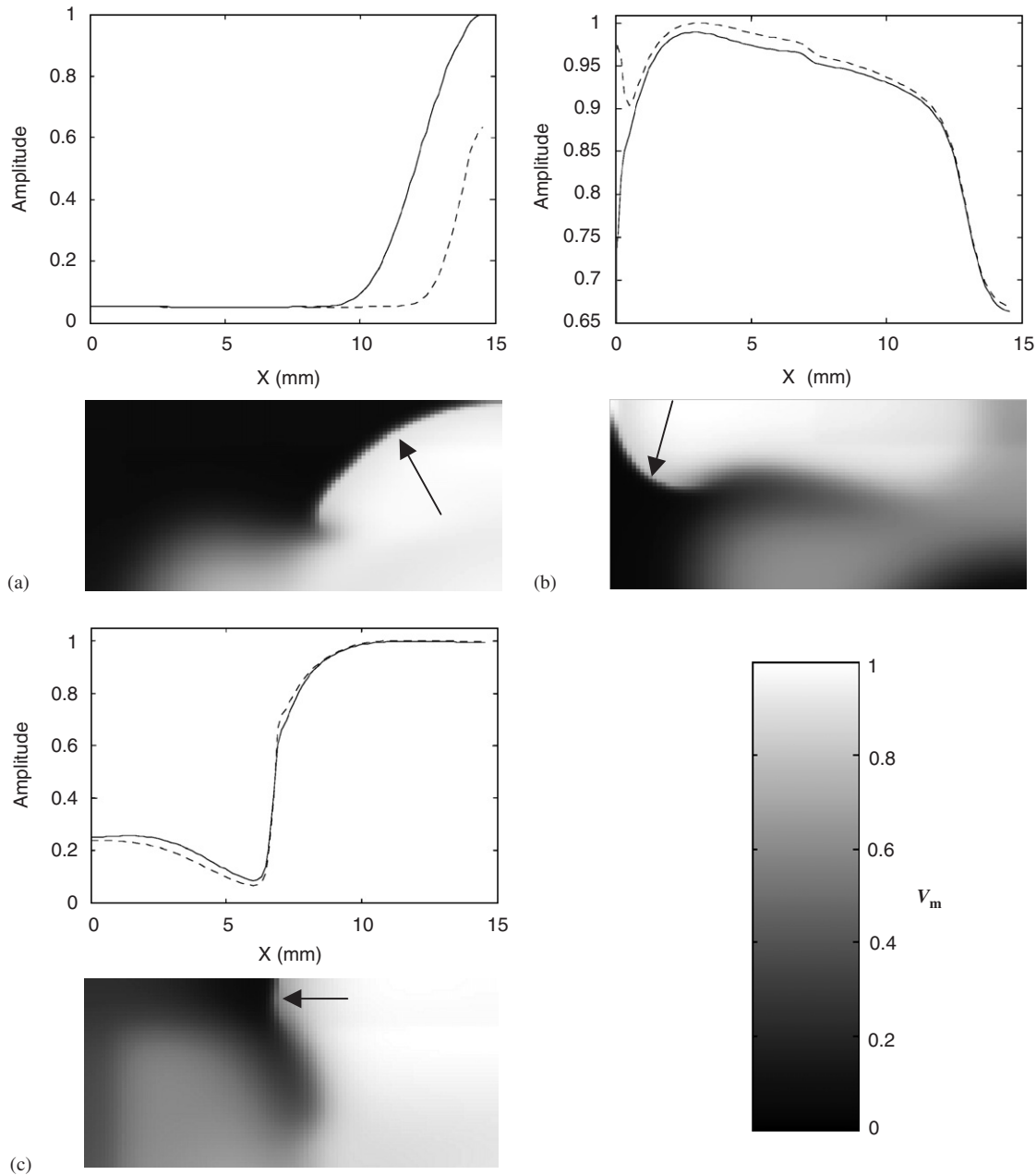
(a)

(b)

(c)

Fig. 3. Traces of the depth-weighted signal (black line) and that of top layer (dotted line) along X-axes with the respective gray-coded images representing the $V_m s$ (data are normalized to the maximum value). The arrowhead shows the direction of the wave front: (a) waves propagate away from the recording surface, (b) waves propagate toward the recording surface, and (c) waves propagate parallel to the recording surface.

model has estimated the non-uniform contributions of different layers to the total fluorescence and the electrical propagation model has given the distribution of the transmembrane potential of electrical waves inside the transmural tissue. The photon transport function we used, including fluence rate $\Phi(z)$ (Eq. (2)) and escape function $G(z)$ (Eq. (3)), are determined by experimental measurement and data fitting by Baxter et al. [4], in which the penetration depths are 0.8 mm for the excitation wavelength (520 ± 30 nm) and 1.34 mm for the emission wavelength (640 ± 50 nm). The probing depth of a fluorescence measurement is usually defined as the depth

above which 90% of the remitted fluorescence originates. The probing depth $Z_{90\%}$ in experiment by Baxter et al. is about 1.202–1.603 mm according to the formula obtained from Welch et at. [17]. The fluence rate and escape function obtained by other experimental measurements can also be used in this model to estimate the effects of the corresponding probing depth. The electrical propagation model does not have any restriction. Any other cardiac ionic models, such as Noble model or Bidomain model, can also be used in order to obtain the distribution of the transmembrane potential during electrical propagation.
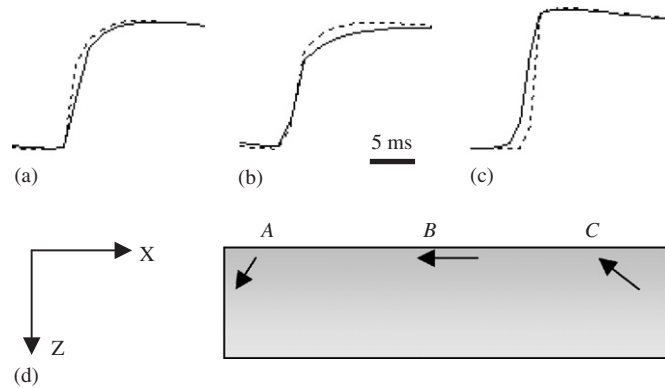
Fig. 4. The upstroke morphology of $\bar{V}$ (black line) and V_0 (dotted line) during a spiral wave at point A, B and C are shown in (a), (b) and (c), respectively. (d) The arrowheads show the directions of wave fronts.

The discrepancy between V_0 and $\bar{V}$ in our research is smaller than that of Janks and Roth [18] who used a bidomain model to calculate and compared the transmembrane potentials of the tissue surface and averaged over depth after a unipolar stimulation on the surface. Their weighting function is based on a simply exponential decay without considering the effect of scattering losses of excitation light on the surface and the attenuation of escape fluorescence. So the profile of their weighting function has a peak at the surface and its attenuation is more slowly than ours. The slowly exponential delay indicates more fluorescence coming from deep layers. So in their study the surface and depth-averaged transmembrane potentials differed by a factor greater than 3, the discrepancy in their study is apparently larger than ours. Our weighting function is based on the results of the experimental measurement and data fitting, so it considers scattering losses of excitation light at the tissue surface. It is maybe a more accurate expression for photon transport in tissue.

Bray et al. [19] simulated the epicardial propagation activity and compared the signal gained from the top epicardial layer with the calculated weighted signal. The time traces of these two signals were differing from ours at repolarizing phase that their depth-weighted signal was lower than that of top epicardial layer. The tissue model we used including some M cells whose APDs are relatively longer (30–40 ms) compared with cells of epicardium and endocardium [16]. It is the reason that $\bar{V}$ is higher than V_0 at repolarizing phase in our simulation and it prolongs the APD of depth-weighted signal. Our three-layer myocardium (endocardium, midmyocardial cell and epicardium) would be more consistent with the realistic myocardium.

Bernus et al. [20] used the photon diffusion equation to simulate the photon transport in the tissue. Comparing with their model, our model is simpler and incorporated light attenuation of excitation light and emission fluorescence. Although our photon transport model does not take into account photon lateral scattering in tissue, the probing depth of an epi-illumination mode we studied is only about 1–2 mm and photon scattering effect could be neglected.

Girouard et al. [9] showed that the optical action potential upstroke can be blurred and lead to a prolongation of the APD because the optical signal is generated from an aggregate of cells within a pixel. According to our simulation, burring would also obviously increased by the depth effect especially during a spiral wave.

5. Summary

Our two-stage model, a model of cardiac electrical activity combined with a photon transport model, has examined the effects of fluorescence coming from a probing depth. It shows that depth-weighted optical signal is different from the signal only on the top layer of tissue. The maximal discrepancy in amplitude between the two signals would be used effectively for core identification. The upstroke morphology of depth-weighted optical signal is obviously dependent upon the propagation direction. The intramural long-APD M cells in tissue would influence the repolarization trace of depth-weighted optical signal causing the prolongation of whole APD.

It is important to note that other factors, such as the geometry of preparation, optical heterogeneities of tissue, photobleaching, also affect the depth-dependent optical signal. But it is too difficult to quantify their effects. This is the first step to quantitatively characterize the optical signal in cardiac optical mapping. We will extend the current work to three-dimensional electrical propagation with an intramural scroll wave. The examination of depth effects of optical signal can provide more information about the intramural cardiac activity and to further investigate complex cardiac spatio-temporal electrodynamics.

References

[1] Z.J. Zheng, J.B. Croft, W.H. Giles, G.A. Mensah, Sudden cardiac death in the United States, 1989 to 1998, Circulation 104 (2001) 2158–2163.

[2] D.J. Christini, L. Glass, Introduction: mapping and control of complex cardiac arrhythmias, Am. Inst. Phys. 12 (2002) 732–739.

[3] I.R. Efimov, Y.N. Cheng, Optical mapping of cardiac stimulation: fluorescent imaging with a photodiode array, Quantitative Cardiac Electrophysiology, Marcel Dekker Inc, New York, 2002, pp. 583–621.

[4] W.T. Baxter, S.F. Mironov, A.V. Zaitsev, J. Jalife, A.M. Pertsov, Visualizing excitation waves inside cardiac muscle using transillumination, Biophys. J. 80 (2001) 516–530.

[5] I.R. Efimov, T.N. Mazgalev, High-resolution three-dimensional fluorescent imaging reveals multiplayer conduction pattern in atrioventricular node, Circulation 98 (1998) 54–57.

[6] Z.H. Xu, Z.X. Zhang, J. Wang, Y.C. Huang, The high-resolution optical mapping of cardiac electrical activity, The Third International Conference on Photonics and Imaging in Biology and Medicine, Wuhan, 2003, pp. 452–456.

[7] B.J. Roth, Artifacs, assumptions, and ambiguity: pitfalls in comparing experimental results to numerical simulations when studying electrical stimulation of the heart, Chaos 12 (2002) 973–981.

[8] B.R. Chio, G. Salama, Optical mapping of atroventricular node reveals a conduction barrier between atrial and nodal cells, Am. J. Physiol. 274 (1998) 829–845.

[9] S.D. Girouard, K.R. Laurita, D.S. Rosenbaum, Unique properties of cardiac action potentials recorded with voltage-sensitive dyes, J. Cardiovasc. Electrophysiol. 7 (1996) 1024–1038.

[10] S.B. Knisley, Transmembrane voltage changes during unipolar stimulation of rabbit ventricle, Circ. Res. 77 (1995) 1229–1239.

[11] L. Ding, R. Splinter, S.B. Knisley, Quantifying spatial localization of optical mapping using Monte Carlo simulations, IEEE Trans. Biomed. Eng. 48 (2001) 1098–1107.

[12] C.H. Luo, Y. Rudy, A model of the ventricular cardiac action potential, depolarization, repolarization, and their interaction, Circ. Res. 68 (1991) 1501–1526.

[13] C.M. Gardner, S.L. Jacques, A.J. welch, Light transport in tissue: accurate expressions for one-dimensional fluence rate and escape function based upon Monte Carlo simulation, Lasers Surg. Med. 18 (1996) 129–138.

[14] Z.L. Qu, A. Garfinkel, An advanced algorithm for solving partial differential equation in cardiac conduction, IEEE Trans. Biomed. Eng. 46 (1999) 1166–1168.

[15] Y.B. Jin, L. Yang, H. Zhang, Y.H. Kuo, Y.Z. Huang, D.Z. Jiang, Numerical algorithm for conduction of action potential in two dimensional cardiac ventricle tissue, J. Xi'an Jiaotong Univ. 38 (2004) 851–854.

[16] D.S. Rosenbaum, F.G. Akar, The electrophysiological substrate for reentry: unique insights from high-resolution optical mapping with voltage-sensitive dyes, in: Quantitative Cardiac Electrophysiology, Marcel Dekker Inc., New York, 2002, pp. 555–582.

[17] A.J. Welch, C. Gardner, R. Richards-Kortum, E. Chan, G. Criswell, J. Pfefer, S. Warren, Propagation of fluorescence light, Lasers Surg. Med. 21 (1997) 166–178.

[18] D.L. Janks, B.J. Roth, Average over depth during optical mapping of unipolar stimulation, IEEE Trans. Biomed. Eng. 49 (2002) 1051–1054.

[19] M.A. Bray, J.P. Wikswo, Examination of optical depth effects on fluorescence imaging of cardiac propagation, Biophys. J. 85 (2003) 4134–4145.

[20] O. Bernus, M. Wellner, S.F. Mironov, A.M. Pertsov, Simulation of voltage-sensitive optical signals in three-dimensional slabs of cardiac tissue: application to transillumination and coaxial imaging methods, Phys. Med. Biol. 50 (2005) 215–229.

Zhenghong XU received the M.S. degree in Instrument Science and Technology from Xi'an Jiaotong University, PR China, in 1999. Now she is a candidate for Ph.D. in biomedical engineering and also a lecturer of the School of Electrical Engineering of Xi'an Jiaotong University. Her main research interests include biomedical photonics and electronic application. Her recent research focuses on the study of cardiac optical mapping and forward/inverse solutions.

Zhenxi Zhang received the Ph.D. degree in Biomedical Engineering and Instrumentation from the Xi'an Jiaotong University, PR China, in 1990. He has worked as a Post-Doctorate scholar in the University of Science and Technology of China, Hefei, from 1991 to 1993. Since 1993 and 1998, he is an Associate Professor and a Professor in the Institute of Biomedical Engineering of Xi'an Jiaotong University. He has worked as a Visiting Scientist in FR Germany from June 1977 to October 1979 at the Stuttgart University, from October 1988 to January 1989 at the "GSF-National Research Center for Environment and Health" (GSF-Forschungszentrum fuer Umwelt und Gesundheit), in Muenchen, Germany, from May to December 1996 at the Robert Roessle Cancer Clinic of the Virchow University Clinic of the Humboldt University in Berlin, Germany and from September to December 1999 at the University of Applied Sciences Wilhelmshaven (Fachhochschule Wilhelmshaven), and from September to December 2006 at the University of Applied Sciences Luebeck (Fachhochschule Luebeck), Germany. His basic research interests are focused on studies of tissue optics, tissue diagnostic spectroscopy, laser diffraction spectroscopy, and the development of laser and optics for biomedical engineering.

Yinbin Jin received his master degree of Medicine from Xi'an Jiaotong University, PR China, in 1992. He is currently working for his Ph.D. in the School of Life Science and Technology and also a lecturer of the School of Electrical Engineering of Xi'an Jiaotong University. His special subject is computer simulation study in cardiac electrophysiology.

Jing Wang received his M.S. degree in Biomedical Engineering from Xi'an Jiaotong University, PR China, in 2002. He is a candidate for Ph.D. in the School of Life Science and Technology at the same university. His main research interests include biomedical photonics and biomedical signal processing.